Received: 7 March 2024 | Revised: 10 April 2024 | Accepted: 15 April 2024 | Published online: 28 April 2024

RESEARCH ARTICLE

Archives of Advanced Engineering Science
2025, Vol. 3(4) 274–283
DOI: 10.47852/bonviewAAES42022781

BON VIEW PUBLISHING

Two-Dimensional Multi-scale Modeling of Fixed Bed Adsorption Column Using Computational Fluid Dynamics Simulation

Salman Khan[1], Muhammad Idrees[2], Muhammad Umar Mushtaq[3,*] and Saddam Hussain[2]

[1]*School of Chemistry and Chemical Engineering, Beijing Institute of Technology, China*

[2]*School of Physics, Beijing Institute of Technology, China*

[3]*Institute of Process Engineering, Chinese Academy of Sciences, China*

Abstract: Natural gas has received much attention with low environmental impact in recent decades as a fuel source. Flexible natural gas purification systems with minimal carbon dioxide footprints are growing in need. There are few techniques that base current industrial decontamination systems on among which adsorption is considered to be the promising one. Herein, multi-scale models have advanced to simulate the hydrodynamics and adsorption dynamics of gases in the adsorption column, a mixture of (CO_2 and CH_4). In the current analysis, a two-dimensional (2D) porous media was modeled using CFD multi-scale model. A fixed bed adsorption column was used for the removal of carbon dioxide (CO_2) from methane (CH_4), and the silicate adsorbent adsorption kinetics linear driving force (LDF) model was simulated to describe it. The adsorption phenomena simulation inside the fixed bed using CFD method was implemented, and using user-defined function (UDF) and the user-defined scalar (UDS), porous media concept and the mass transfer coefficient for gas components (CO_2/CH_4) were developed. The experimental data were used to validate the model which was collected based on varying a number of laboratory conditions. The simulation result prediction of methane recovery and breakthrough curves shows an acceptable agreement with the experimental data with the highest error lower than 3.5%. Moreover, the effect of feed concentration (15, 35, and 75%), feed velocity effect (0.03, 0.05, and 0.07 m/s), effect of bed porosity (0.42, 0.52 and 0.62), effect of inlet concentration on temperature (15, 30, and 60%), particle radius (0.0006, 0.0007, and 0.0008 m) and effect of bed height (0.3, 0.4, and 0.5 m) were investigated. The present results received from the CFD approach suggest that they are capable to predict the adsorption phenomena and hydrodynamics in the adsorption column.

Keywords: natural gas adsorption, user defined function (UDF), linear driving force (LDF), computational fluid dynamics (CFD)

1. Introduction

Separation of carbon dioxide (CO_2) from natural gas (methane) is critical for enhancing gas recovery and improving methane production. Highly containing CO_2 amount in the natural gas leads potentially to many shortcomings such as causative contribution to difficult pipeline-corrosion and noticeable fall in the natural gas heating rate [1, 2]. Generally, for natural gas requires pipeline specification of carbon dioxide concentration less than 2–3%. Mostly natural gas contains 0–20% of CO_2 and 70–90% of CH_4. Hence, CH_4 was considered as main representative component of natural gas containing CO_2 as only major impurity in this observation [3–5]. A variety of separation methods (membrane separation, absorption, cryogenic techniques, and solid sorbent adsorption) are in place to minimize CO_2 emissions [6, 7].

Mostly, in adsorption processes, the adsorbent and the fluid are in close contact in a packed bed. Due to low capital expenditure and low-cost energy requirements, technology for pressure swing adsorption (PSA) has gained interest. The conditions required for PSA cycle to be appropriate for the purification of CO_2/CH_4 mixture are to acquire an adsorbent selection of these compounds. A mild adsorption affinity of adsorbent for CO_2 is favorable because too high affinity of adsorbent brings hurdle in the recovery process and hence affects negatively the economy of the selected system [8, 9]. The modeling of the adsorption process is also a key role in order to understand fundamental transport phenomena processed inside the adsorbent. This understanding facilitated by preliminary modeling, enhances the design and optimized adsorption technology [10, 11].

In recent years, a large number of adsorbents, such as silicalite, zeolites, activated carbons, carbon molecular sieves, and metal oxides, have been widely studied for the active removal of CO_2. The selection of adsorbents with high selectivity and outstanding working strength, efficient desorption capability, is the most important consideration for the design of the adsorption-desorption system for effective CO_2 separation [11, 12]. Among all the commercial adsorbents available to carry out this separation on the basis of equilibrium separation, due to the polar characteristics of the adsorbate, zeolites are considered as possible candidates because they are highly selective

*Corresponding author: Muhammad Umar Mushtaq, Institute of Process Engineering, Chinese Academy of Sciences, China. Email: muhammadumarmushtaq@mails.ucas.ac.cn

for CO_2. The separation of H_2/CO_2 and the CO_2/CH_4 was patented using (5A) zeolites [13–15]. Separating CO_2 from the natural gas, a mathematical model was developed to describe Pressure Swing Adsorption (PSA) [16]. Results interpreted and calculated using A Langmuir equilibrium isotherm were in high correlation with the experimental data, approximately 3% error margin [17]. However, the typical CO_2 adsorption of these adsorbents is too heavy, which makes the desorption process difficult. Moreover, the desirable adsorption of CO_2 is accomplished without affecting the performance of the adsorbent in the presence of other impurities in the feed gas, such as sulfur and water content, silicalite and USY are hydrophobic zeolites that show a good compromise between high CO_2 selectivity and easier regeneration with a low aluminum (Al) content [18, 19]. The regeneration rate of CO_2 from these zeolites is therefore a significant value that is more prominent than from the hydrophilic adsorbents, since the interaction is regulated by the quadruple moment of CO_2. In addition, hydrophobic (water-removing) zeolites, unlike their hydrophilic (water-attracting) counterparts, can be substituted in the presence of H_2O moisture in adsorption procedures for CO_2 removal, as their adsorption capacity is not significantly reduced in the former case [20, 21].

Inside fixed bed adsorption column, modeling of equilibrium adsorption phenomenon and kinetics, many attentions and keen interests have been given to embrace cost-effective experimental setup for industrial development [5]. Fixed bed column contains numerous models for mass transfer in order to predict successfully such as linear driving force (LDF) model [5, 22], pore diffusion model (PDM), and homogeneous surface diffusion model (HSDM) [23, 24]. The mathematical forms of PDM and HSDM are more complex and time consuming although these models can achieve the exact results. In contrast, LDF model has been widely applied owing to simplicity and the saving in computational time to successfully calculate the mass shift in preset bed column [25, 26]. Due to that, LDF model by several scientists has been applied to determine kinetics of the desirable CO_2 adsorption in fixed bed column [5]. Under the model assumption set, transferring the mass between two phases of the adsorbate and adsorbent was simulated using the LDF model, including relatively minimal pressure drop, both axially and radially. The removal of CO_2 is also investigated via PSA [27–30]. Following LDF model, the numerical simulation was performed to describe the kinetic of adsorption. The investigated results were in close agreement as predicted by the model and a considerable amount of NO_2 gas was recovered. There has recently been a lot of interest in integrating engineering models with rigorously simulated instruments that lead to the remarkable developments in computational resources and codes [31–33]. Simulation methods offer a potentially more attractive substitute to expensive and the time-wasting experimentation. Computational fluid dynamics (CFD) is properly applied when process efficiency is calculated by using fluid dynamics. CFD approach has been commonly proposed as consistent technique for mass and heat transfer phenomena to simulate and model hydrodynamic design and optimization of process equipment [33, 34]. However, the CFD investigations implicated to the fixed bed adsorption have been established to be limited. Therefore, in the packed bed carbon dioxide adsorption column, the applicability of CFDs to simulate adsorption and transport processes mechanisms is promising.

In this current work, a model is to be tested, and the CO_2 and CH_4 mixtures hydrodynamics and adsorption phenomena are simulated in a column of filled fixed bed adsorption silicalite. The impacts of various operating variables such as inlet concentration, fluid flow rate, particle radius, bed porosity, and temperature impact on inlet concentration on the breakthrough curve are considered. Additionally, a novel aspect of this study is the incorporation of a novelty point, where the breakthrough curve is analyzed in terms of a unique parameter or condition that has not been explored extensively in previous research. This novelty point could provide valuable insights into the behavior of the adsorption system and offer new perspectives for optimization or further research.

2. Mathematical Modeling

2.1. CFD modeling

For the packed bed column, it has developed the 2D porous media CFD model. Under normal conditions, carbon dioxide (CO_2) and methane (CH_4) were selected as the feed gas mixture at a concentration of 50 percent v/v. The adsorbent within the bed is considered a porous medium, so in the simulation of fluid flow, a technique has been used in the packed bed of porous medium. The design of a generalized model for the adsorption mechanism was set according to the criteria.

1) Compressibility of fluid is usually neglected and the gas phase is considered as compressible.
2) CO_2 and CH_4 are assumed to have competitive adsorption behavior.
3) The mass transfer rate during the adsorption phase was calculated using the LDF model.
4) Wherever the porosity is considered as uniform, porous media domain is used throughout.
5) The coefficient of mass transfer is conglomerate of the macro pore diffusion and external fluid film resistance.
6) Within bed, heat transfer is neglected.

Simulations are performed using fluent tools incorporated into Ansys Workbench 16. Governance and additional equations are used in the mathematical model. Continuity equation, Navier-Stokes equation, mass balance equation, porous medium momentum source term, energy balance equation, and additional Langmuir Isotherm equations are included in the governing equations.

2.2.1. Governing equations

Equation of continuity:

The equation for continuity is,

$$\frac{\partial \rho}{\partial t} + \frac{\partial (\rho u)}{\partial x} + \frac{\partial (\rho v)}{\partial y} = 0 \tag{1}$$

Navier-stokes equations:

The conventional fluid Navier-Stokes equation by introducing a porous medium momentum source "Si" to describe the exact performance of porous media is updated. The equation is represented as:

Navier-stokes equation in x-direction:

$$\frac{\partial (\rho u)}{\partial t} + \frac{\partial (\rho u u)}{\partial x} + \frac{\partial (\rho v u)}{\partial y} = -\frac{\partial P}{\partial x} + \frac{2\partial}{\partial x}\left(\frac{\mu \partial u}{\partial x}\right) - \frac{2}{3}\frac{\partial}{\partial x}\left[\mu\left(\frac{\partial u}{\partial x} + \frac{\partial v}{\partial y}\right)\right] + \frac{\partial}{\partial y}\left[\mu\left(\frac{\partial u}{\partial y} + \frac{\partial v}{\partial x}\right)\right] + \mathrm{Si}_x \tag{2}$$

Navier-stokes equation in y-direction:

$$\frac{\partial(\rho v)}{\partial t}+\frac{\partial(\rho vv)}{\partial y}+\frac{\partial(\rho vu)}{\partial x}=-\frac{\partial P}{\partial x}+\frac{2\partial}{\partial y}\left(\frac{\mu\partial v}{\partial y}\right)-\frac{2}{3}\frac{\partial}{\partial y}\left[\mu\left(\frac{\partial u}{\partial x}+\frac{\partial v}{\partial y}\right)\right]+\frac{\partial}{\partial x}\left[\mu\left(\frac{\partial u}{\partial y}+\frac{\partial v}{\partial x}\right)\right]+\mathrm{Si}_y \quad (3)$$

u and v are velocity in x and y directions, ρ and μ are the density and viscosity. Viscosity and inertial losses are based on the Ergun equation and are included in the "Si" porous medium source definition. Where C_2 (m^{-1}) is the coefficient of inertial resistance t and alpha (m^{-2}) is the coefficient of viscous resistance, the following is the case:

$$\mathrm{Si}=\frac{\mu}{\alpha}u_i+\mathrm{C}_2\left(\frac{1}{2}\rho u_i|u_i|\right) \quad (4)$$

$$\mathrm{C}_2=\frac{1.75}{D_{pt}}\frac{(1-\varepsilon)}{\varepsilon^3}\ ,\ \alpha=\frac{{D_{pt}}^2}{150}\frac{\varepsilon^3}{(1-\varepsilon)^2} \quad (5)$$

Gases mass balance equation:

The scale of mass transfer between absorbent particle (bulk) and the scale of mass transfer inside adsorbent particles are two separate scales at which the transfer of material in the adsorption unit can be studied.

$$-D_{CDi}\frac{\partial^2 C_g}{\partial x^2}+\frac{\partial uC_g}{\partial x}+D_{CDi}\frac{\partial^2 C_g}{\partial y^2}+\frac{\partial vC_g}{\partial y}+\frac{\partial C_g}{\partial t}+\left[\frac{1-\varepsilon}{\varepsilon}\right]\rho_p\frac{\partial q_g}{\partial t}=0 \quad (6)$$

The adsorption rate $\left(\frac{\partial q_g}{\partial t}\right)$ was obtained from Linear driving force (LDF).

Mass transfer model:

$$\rho_p\frac{\partial q_g}{\partial t}=k_i a(q_i^*-q_i) \quad (7)$$

"a" is the surface area, "ρ_p" particle density, "k_i" is the average mass transfer coefficient. where "q_i" is the bulk gas concentration and "q_i*"is pellet concentration which is described by multi-component Langmuir isotherm.

$$k_i=\left(\frac{D_{md}}{2R_{pt}}\right)*(1.85((1-\varepsilon)/\varepsilon)^{0.33})Sc^{0.33}Re^{0.33} \quad (8)$$

where the Schmidt numbers S_C, the Reynolds number Re, D_{md} is the molecular diffusivity and R_{pt} is the pellet radius.

$$D_{CDi}=0.7D_{md}+uR_{pt} \quad (9)$$

D_{CD} is the column dispersion coefficient.

$$D_{md}=1.8583\times10^{-3}\times\frac{T^{\frac{3}{2}}\left(\frac{1}{M_{CO2}}+\frac{1}{M_{CH4}}\right)^{\frac{1}{2}}}{P{\sigma^2}_{AB}\Omega_{AB}} \quad (10)$$

where Ω is the Collision integral, σ_{AB} is the Lennard-Jones Constant.

Equation of energy:

The total energy equilibrium for the column bulk flow calculating the heat produced by adsorption:

$$\rho_g C_{pg}\frac{\partial T}{\partial t}+\varepsilon\rho_g C_{pg}\left[u\frac{\partial T}{\partial x}+v\frac{\partial T}{\partial y}\right]-K_L\left[\frac{\partial^2 T}{\partial x^2}+\frac{\partial^2 T}{\partial y^2}\right]=-\rho_g(\Delta H_i^*)\sum_{i=1}^{N}\frac{\partial q_g}{\partial t} \quad (11)$$

The thermal conductivity (W/m. K) is K_L, density is ρ_g, heat capacity is C_{pg} and the adsorption heat is H_i* (kJ mol^{-1}).

2.1.2. Additional equations

$$q_i^*=\frac{q_s K_{eqi}C_A}{1+K_{eqi}C_A+K_{eqi}C_B} \quad (12)$$

Mean adsorbed concentration (kg m^{-3}) is q_i^*, and the concentration of adsorbent energy is qs as in Equation (12). By estimating the pellet concentration of q_i* with respect to the contact among two components by using the Langmuir multi-component model, Equations (6), (7), and (12) are combined to solve the mass balance of the column. To evaluate the equilibrium constant of K_{eqi}, the Vant-Hoff correlation was applied.

$$K_{eqi}=K_0\exp\left(\frac{-\Delta H_i}{RT}\right) \quad (13)$$

where $K_0=0.0206$ is the pre-exponential factor, ΔH_i is the heat of adsorption.

$$C_i=\frac{y_i P}{RT_g} \quad (14)$$

where C_i is the Concentration, y_i is the mass fraction.

2.2. Numerical solution

The particles are known as a continuous porous medium for the adsorbent to show the adsorption mechanism (actual), and viscous resistance and inertial resistance are two coefficient that are added to the CFD to reflect flow resistance. For the above CFD model eq., utilizing the finite volume approach, the numerical solution can be found using Fluent 16 software. The laminar fluid flow was simulated by Ansys Fluent built-in solver in porous silicalite. For other transport equations, such as concentrations of CO_2 and CH_4, average transfer of mass to the adsorbent particles, and temperature of the gas, user-defined functions (UDFs) were used along with user-defined scalars (UDS) in the Ansys Fluent utility. For the correlation of velocity and pressure, a SIMPLE algorithm is used. To calculate the flow variables, first-order discretization schemes are used. For all variables, convergence criteria are set at 10^{-5}. A silicalite-filled packed bed column was considered in the present analysis. Figure 1 shows the schematics of the fixed bed adsorption column. To save computational time, the Gambit software was used for geometry and meshing which have the inner diameter of 38 mm and 500 mm in length. In order to distinguish the fixed bed domain, structural quadrilateral grid was used.

Figure 1
Schematics of fixed bed adsorption column

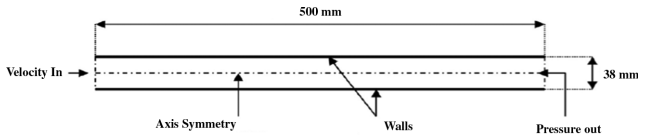

2.3. Grid independence test

To validate the preciseness of CFD results, mesh independency is one of the methods utilized. Without the mesh independence test, CFD simulation results are unreliable. Therefore, at two various grid sizes, i.e., grid 1 quadrilateral cells 2890, and grid 2 the quadrilateral cells 4651 that used for further studies, the mesh independency test was conducted. Carbon dioxide concentration at the outlet was used to find out the mesh number effect with time, as shown in Figure 2. It is known that the outlet concentration of carbon dioxide is effected in small numbers by the mesh numbers, which may be due to the reason of the premise of having homogeneous porous media and thus by putting in two resistances, the inertial resistance loss and viscous resistance loss. Mass source term narrating transport of carbon dioxide by the adsorbent is also counted in.

Figure 2
Effect of mesh number on breakthrough curve

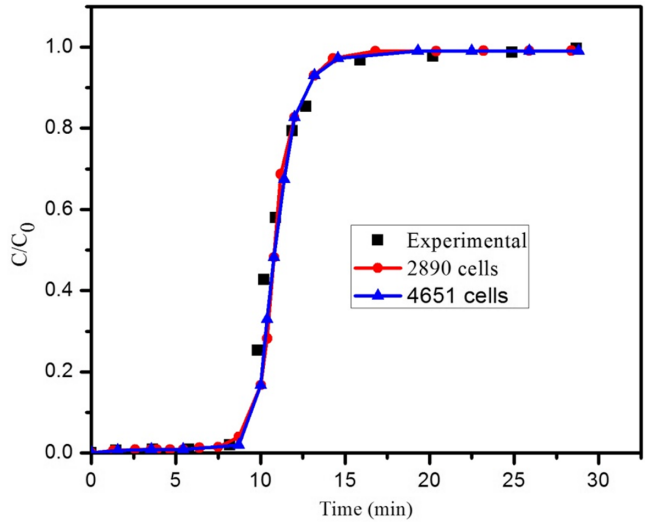

2.4. Boundary conditions

In the current study, at the inlet of the adsorption column, the velocity was kept precise. As Table 1 shows the properties of adsorbent and geometry condition with boundary, there was a mixture in the gaseous phase, and the species' velocity and mass were defined under the entry boundary conditions. The pressure was defined at the outlet. Similarly, at outlet boundary conditions, the gauge pressure and mass fraction of the species were indicated. In addition, there was no slip shear condition considered for the fixed bed column wall. The model was given conditions which were then employed to promote the fusion of the simulation. The surrounding temperature was set at 300 K, and the set-off pressure was calibrated at 101,325 kPa. Axial velocity was initially described at contrasting input speeds, and the radial velocity was set at zero. The initial conditions are as follows:

$$\begin{aligned} C_1(x,y) \text{ at } (t=0) &= C_0 \\ u(x,y) \text{ at } (t=0) &= 0 \\ v(x,y) \text{ at } (t=0) &= 0 \\ q_1(x,y) \text{ at } (t=0) &= q_0 \\ T(x,y) \text{ at } (t=0) &= T_0 \\ P(x,y) \text{ at } (t=0) &= P_0 \end{aligned} \tag{15}$$

Table 1
Properties of adsorbent, geometry and simulation boundary conditions

Adsorbent properties	
Type	Silicalite
Porosity	0.59
Bulk density (kg/m^3)	1070
Adsorption columns	
Inside diameter (m)	0.038
Outside diameter (m)	0.045
Bed length (m)	0.5
Bed porosity	0.52
Particle radius (m)	0.0007
Equilibrium data for CO_2 adsorption	
Temperature (K)	300
Pressure (bar)	1–60
Maximum capacity (q_s mol/kg)	4.79
Simulation boundary conditions	
Pressure (bar)	1–60
Inlet temperature (K)	300
Inlet velocity (m/sec)	0.05
Inlet CO_2 mass fraction	0.5
Inlet CH_4 mass fraction	0.5

2.5. Validation of model

Model differentiation of simulation and experimental values. The CO_2 concentration outflow at the column was taken into account by the simulation model for various run circumstances at various periods. The outcomes were simulated using FLUENT 16 and differentiated with experimental data. The simulated data indicate a fairly strong alignment, based on the observations, of experimental data with the highest error lower than 3.5%. Good accordance-based model outcomes, many parameters (feed quality, bed porosity, and feed velocity effects on temperature and particle radius) were analyzed which effects the adsorption capacity of CO_2. The validation of CFD model by comparing it with experimental data was obtained based on the breakthrough curve. Figures 3 and 4 display combined uptake data for kinetic CO_2 and CH_4 adsorption, respectively. Simulation data was assessed on the basis of the experimental parameters shown in Table 1. It took 8 min for the simulations to get the bed saturated.

Figure 3
Comparison of CO_2 simulation and the experimental breakthrough curve

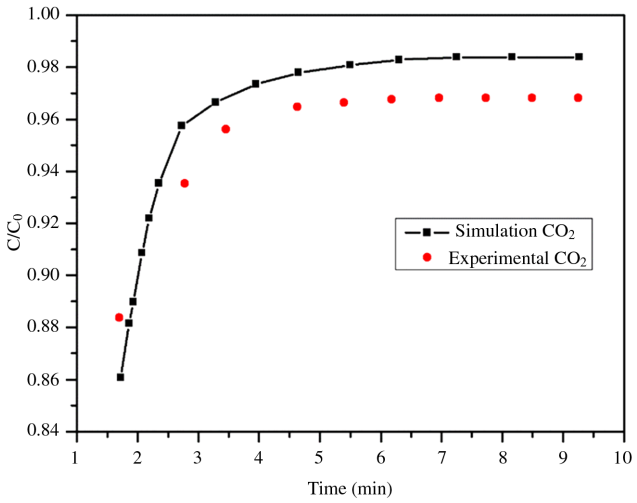

Figure 4
Comparison of CH_4 simulation and experimental breakthrough curve

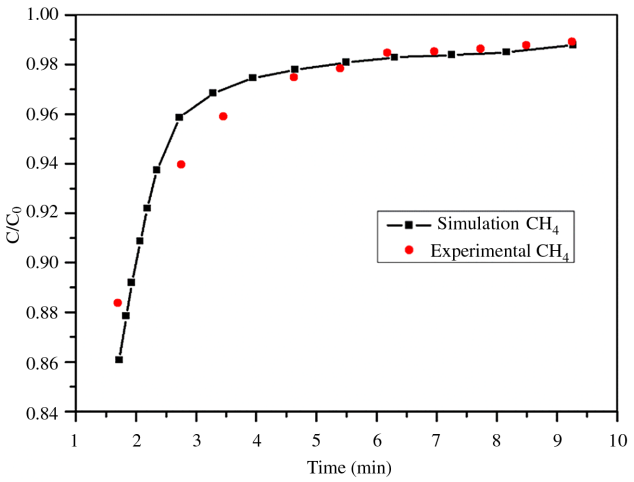

3. Findings and Discussion

3.1. Effect of CO_2 concentration

Effect of CO_2 concentration as in Figure 5 shows that inside adsorption column at variating durations (0.5, 5, 10 mint) was assessed and to analyze the adsorption capacity three divergent quantities (15%, 35%, and 75%) of CO_2 were utilized, the adsorption capacity can be inferred from CO_2 concentration factor, where higher concentration front is associated with reduced adsorption efficacy. In the adsorption column with 15 percent of the CO_2 feed, a rapid build-up of the CO_2 concentration front was observed with (from 0.5 to 5 mint). As the adsorption process continues for 10 min, fixed bed adsorption procedure tends to give a similar CO_2 concentration factor in the column. At the start of the adsorption time, the rapid increase in bed concentration (0.5 to 5 min) was due to the high compatibility of the physical

Figure 5
Effect of inlet concentration on the simulated adsorption process

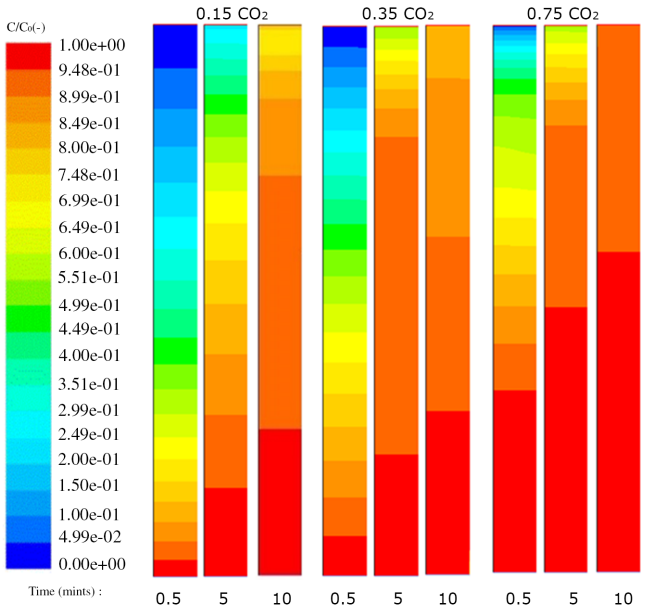

Vander Waals and electrostatic forces of the fresh adsorbent to adsorb. The capacity of adsorbent decreases when the bed turns into saturated as the adsorption process continues towards the balance. For the fully packed column bed under each of the investigated adsorption cycle, it appears to have a greater CO_2 concentration when comparing the concentration of CO_2 feed (75%) with other situations. These findings demonstrated that increasing CO_2 feed generally results in a faster reach of bed saturation and equilibrium.

3.2. Effect on feed velocity

The feed velocity effect on CO_2 adsorption under different feed velocities as in Figure 6 in the fixed bed adsorption column, 0.03, 0.05, 0.07 m sec^{-1} The CO_2 intake concentration remained constant at 50 percent. According to figure as the velocity rises,

Figure 6
The simulations breakthrough curve and the impact of inlet velocity

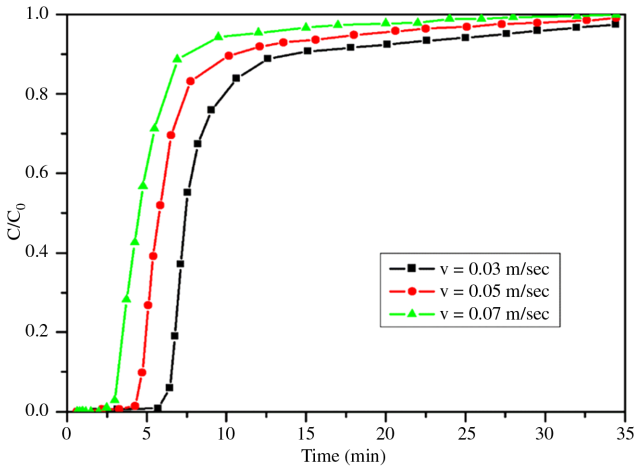

the breakthrough curve becomes steeper. This shows that the commodity is generated under different feed velocities at a higher CO_2 concentration. The gas mixture shortens the residence cycle at higher feed velocity. These phenomena can be explained by the reduction of residence time of CO_2 in the column at higher feed velocity. Small residence time directly decreases mass transfer of the CO_2 from bulk flow to the absorbent (silicalite) which subsequently reduces the adsorption rate.

3.3. Effect of particle radius

Particle size effect on the effluent concentration as Figure 7 presented. Other parameters such as flow rate and bed porosity were kept constant during these simulations. The steepness of the breakthrough curves decreases with the consistent increase in particle size from 0.0006 to 0.0008 m. The overall length of the path within the pore also increases, and the particles in which the stagnant film resides increase their thickness as the particle's diameter increases. The overall kinetics of the process are now moderate in these circumstances, since the time to reach the adsorbate molecules at their adsorption sites is longer as the diffusion path along the pores is high.

Figure 7
Effect of particle radius on simulated breakthrough curve

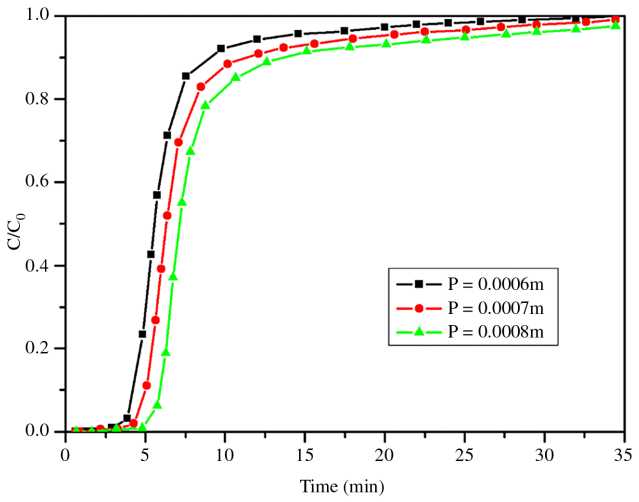

3.4. Effect of bed porosity

Under different bed porosity as Figure 8 shows, the effect on breakthrough curves, of the bed porosity. As bed porosity increases, i.e., 0.42, 0.52, 0.62, at the outlet the CO_2 concentration will be higher. This shows that as bed porosity increases, less CO_2 can be removed, resulting in increased CO_2 concentration at the column exit. These phenomena are defined by the fluid flow and its effect through a packed bed. The pressure difference and velocity values are being effected much by the packing of the bed. The lower the bed's porosity, the greater the velocity, and the lower the bed's gas residence time. This will offer a larger CO_2 concentration to the commodity stream. Since lower bed porosity, however, leads towards increment in the rate of adsorption and decrement in concentration of CO_2 at the outlet, the porosity, based on mass balance equations, has a flip effect. The effect of

Figure 8
Effect of bed porosity on the column outlet breakthrough curve in a simulation

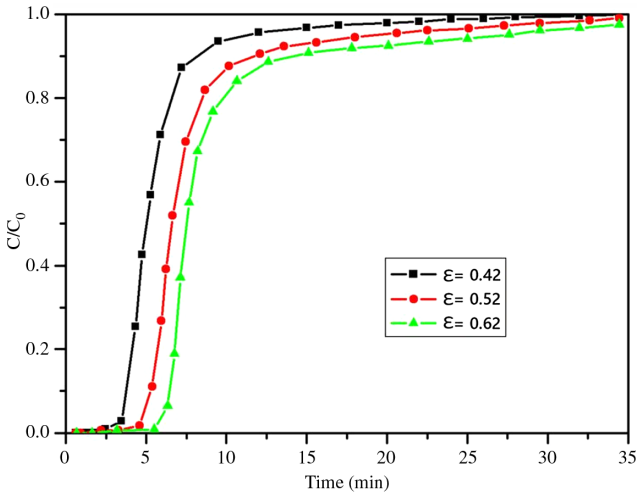

hydrodynamics on the mass transfer effect of CO_2 adsorption using the fixed bed adsorption column can therefore be estimated to be more relevant on the basis of Figure 8.

3.5. Effect of CO_2 concentration on temperature

The formation of the temperature profiles at different levels of CO_2 (15, 30, 60%) as Figure 9 reflects. At the column outlet, the temperature profiles were checked. Due to the exothermic nature of CO_2 adsorption, the column temperature tends to increase as CO_2 concentration increases. This is exemplified in Figure 9, where initial temperature of the column (286 K) has been observed to increase over the entire adsorption duration from 286 to 296 K, 310 and 319 K, respectively, at 15, 30, and 60 percent of the CO_2 concentration. This reality is because of the direct relationship between the quantity adsorbed and the released temperature. The CO_2 adsorption rate is higher for each

Figure 9
Different inlet concentration effects on the temperature profile at the outlet of the column

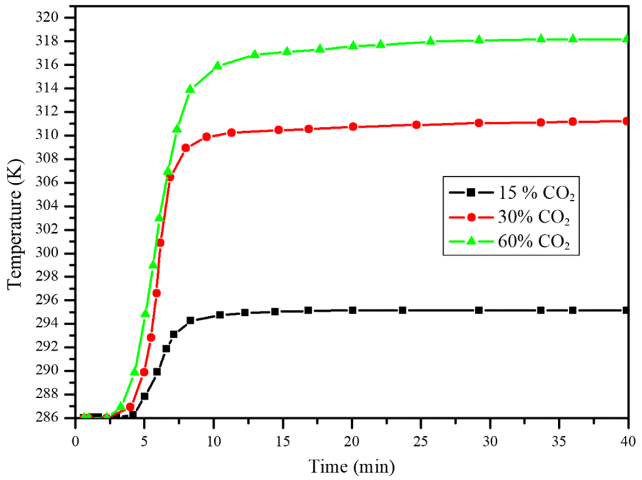

concentration given at the beginning of adsorption (<<20 min), when the temperature increment gradient is higher. The temperature gradient hits the established stage when the adsorption time exceeds 20 min, where further changes are comparatively small in comparison with adsorption time. This is a result of adsorbent bed's CO_2 saturation.

3.6. Effect of bed height

The effects of varied bed heights (0.3, 0.4, and 0.5 m) on the breakthrough curve recorded at the fixed bed outlet as in Figure 10 illustrates. More time for breakthroughs results in higher column bed height. Both numerical (solid lines) and experimental (symbols) results are reported. Greater column bed height increases the amount of time it takes for the complete column to reach saturation in comparison to other column bed heights. The longer duration from the break-point to saturation also occurs at higher bed heights which could disperse deeper inside the particle due to the longer residence time compared to the lower bed height.

Figure 10
Bed height impact on breakthrough curve

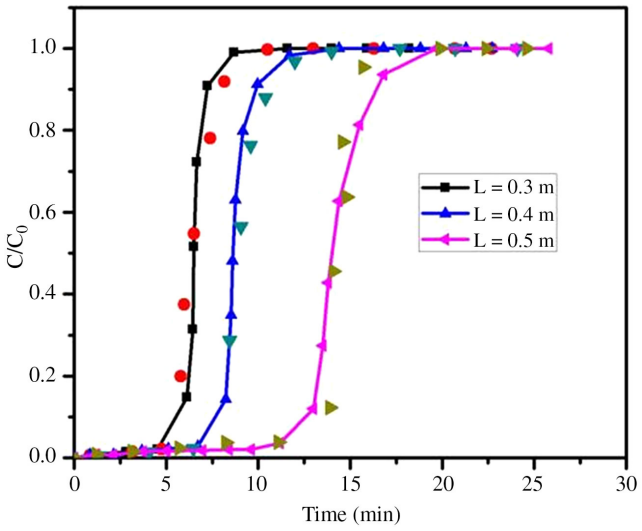

3.7. Methane recovery

The valuation of the Pressure Swing Adsorption (PSA) process enactment was measured based on the recovery of the desired (methane) product as Figure 11 demonstrates. Recovery can be considered as follows:

$$\text{Recovery } (\%) = \frac{\text{Methane } (CH_4) \text{ out from the column}}{\text{Methane } (CH_4) \text{ enter the column}} \times 100\% \quad (16)$$

The recovery of product curve is plotted as function of carbon dioxide (CO_2) feed concentration at a constant flow rate of 0.05 m/s and pressure of 2×10^6 Pa. The result shows that the methane (CH_4) recovery compacts at high CO_2 feed concentration. Under condition of reduced carbon dioxide (CO_2) feed concentration, there is corresponding increase methane (CH_4) feed concentration. The amount of unabsorbed methane (CH_4) after breakthrough

Figure 11
Comparison of simulation and experimental recovery of methane at different CO_2 concentration

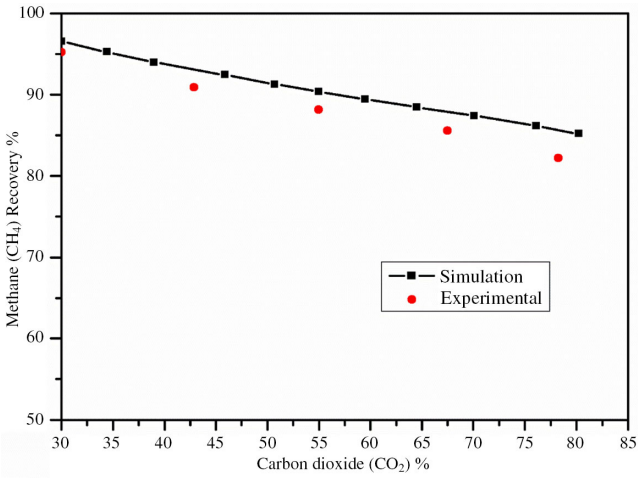

time is higher since there are higher concentrations of methane (CH_4) in feed, which increases the recovery of methane (CH_4). Through higher carbon dioxide (CO_2) feed concentration (corresponding lower methane (CH_4) feed concentration), the amount of unabsorbed methane (CH_4) after breakthrough time is lower since there is lower concentration of methane (CH_4) in the feed, which decreases the recovery of methane (CH_4). The results of this study show that silicalite presented a high adsorption attraction towards both carbon dioxide (CO_2) and methane (CH_4). Comparison between the experiment and simulation recoveries were obtained with maximum error of less than 9%. The errors might be due to the segregation of adsorption heat and heat transfer within the bed in the explanation of the governing equations.

4. Conclusion

A two-dimensional (2D) multi-scale model of carbon dioxide (CO_2) and methane (CH_4) adsorption on silicalite pellets in a fixed bed was taken into account. As well as different mass transfer mechanisms, various models have been checked for gas-solid adsorption balance. For adsorption kinetics, the breakthrough curves of methane (CH_4) and CO_2 were effectively represented by a model using the LDF approximation. The model also well forecasted the breakthrough curves obtained with gaseous mixtures of CO_2 and CH_4. A number of equation add-on user-specific functions (UDFs) and scalar transport equations (UDSs) have been developed in C language, which can be combined to calculate molar and fluid and porous bed temperatures with the ANSYS-Fluent solver, adsorbed CO_2 and CH_4 concentrations. The validation was carried out with experimental hydrodynamics data and mass transfer models. The simulation of the CH_4 recovery using the CFD method reveals fair agreement with the experimental values. Several significant operating parameters were considered in this study and the results showed a fair way of affecting feed concentration, feed velocity, particle radius, temperature inlet concentration, bed height effect, and bed porosity. The current investigation also demonstrated that the effectiveness and capacity of the adsorption process were significantly influenced by the hydrodynamics within the packed beds. Further investigations building upon these findings can lead to advancements in process optimization, material design, and environmental sustainability.

Ethical Statement

This study does not contain any studies with human or animal subjects performed by any of the authors.

Conflicts of Interest

The authors declare that they have no conflicts of interest to this work.

Data Availability Statement

Data are available from the corresponding author upon reasonable request.

Author Contribution Statement

Salman Khan: Conceptualization, Methodology, Software, Investigation, Resources, Writing – original draft, Supervision. **Muhammad Idrees:** Software, Investigation, Writing – original draft. **Muhammad Umar Mushtaq:** Validation, Data curation, Visualization, Project administration. **Saddam Hussain:** Formal analysis, Data curation, Writing – review & editing.

References

[1] Gomes, V. G., & Yee, K. W. K. (2002). Pressure swing adsorption for carbon dioxide sequestration from exhaust gases. *Separation and Purification Technology*, *28*(2), 161–171. https://doi.org/10.1016/S1383-5866(02)00064-3

[2] Grande, C. A., Cavenati, S., Barcia, P., Hammer, J., Fritz, H. G., & Rodrigues, A. E. (2006). Adsorption of propane and propylene in zeolite 4A honeycomb monolith. *Chemical Engineering Science*, *61*(10), 3053–3067. https://doi.org/10.1016/j.ces.2005.11.058

[3] Dantas, T. L. P., Luna, F. M. T., Silva, I. J., Torres, A. E. B., de Azevedo, D. C. S., Rodrigues, A. E., & Moreira, R. F. P. M. (2011). Modeling of the fixed-bed adsorption of carbon dioxide and a carbon dioxide-nitrogen mixture on zeolite 13X. *Brazilian Journal of Chemical Engineering*, *28*(3), 533–544. https://doi.org/10.1590/S0104-66322011000300018

[4] Nouh, S. A., Lau, K. K., & Shariff, A. M. (2010). Modeling and simulation of fixed bed adsorption column using integrated CFD approach. *Journal of Applied Sciences*, *10*(24), 3229–3235. https://doi.org/10.3923/jas.2010.3229.3235

[5] Delgado, J. A., Uguina, M. A., Sotelo, J. L., Ruíz, B., & Rosário, M. (2007). Separation of carbon dioxide/methane mixtures by adsorption on a basic resin. *Adsorption*, *13*(3–4), 373–383. https://doi.org/10.1007/s10450-007-9020-x

[6] Grande, C. A., Blom, R., Möller, A., & Möllmer, J. (2013). High-pressure separation of CH_4/CO_2 using activated carbon. *Chemical Engineering Science*, *89*, 10–20. https://doi.org/10.1016/j.ces.2012.11.024

[7] Cen, P., & Yang, R. T. (1985). Separation of a five-component gas mixture by pressure swing adsorption. *Separation Science and Technology*, *20*(9–10), 725–747. https://doi.org/10.1080/01496398508060701

[8] Chang, D., Min, J., Moon, K., Park, Y. K., Jeon, J. K., & Ihm, S. K. (2004). Robust numerical simulation of pressure swing adsorption process with strong adsorbate CO_2. *Chemical Engineering Science*, *59*(13), 2715–2725. https://doi.org/10.1016/j.ces.2004.01.067

[9] Serna-Guerrero, R., & Sayari, A. (2010). Modeling adsorption of CO_2 on amine-functionalized mesoporous silica. 2: Kinetics and breakthrough curves. *Chemical Engineering Journal*, *161*(1–2), 182–190. https://doi.org/10.1016/j.cej.2010.04.042

[10] Chue, K. T., Kim, J. N., Yoo, Y. J., Cho, S. H., & Yang, R. T. (1995). Comparison of activated carbon and zeolite 13X for CO_2 recovery from flue gas by pressure swing adsorption. *Industrial & Engineering Chemistry Research*, *34*(2), 591–598.

[11] Kapoor, A., & Yang, R. T. (1989). Kinetic separation of methane—carbon dioxide mixture by adsorption on molecular sieve carbon. *Chemical Engineering Science*, *44*(8), 1723–1733. https://doi.org/10.1016/0009-2509(89)80014-4

[12] Shafeeyan, M. S., Wan Daud, W. M. A., & Shamiri, A. (2014). A review of mathematical modeling of fixed-bed columns for carbon dioxide adsorption. *Chemical Engineering Research and Design*, *92*(5), 961–988.

[13] Sircar, S., & Zondlo, J. W. (1978). *Separation of multicomponent gas mixtures* (U.S. Patent No. US4171206A). Google Patents. https://patents.google.com/patent/US4171206A/en

[14] Dunne, J. A., Mariwala, R., Rao, M., Sircar, S., Gorte, R. J., & Myers, A. L. (1996). Calorimetric heats of adsorption and adsorption isotherms. 1. O_2, N_2, Ar, CO_2, CH_4, C_2H_6, and SF_6 on silicalite. *Langmuir*, *12*(24), 5888–5895. https://doi.org/10.1021/la960495z

[15] Golden, T. C., & Sircar, S. (1994). Gas adsorption on silicalite. *Journal of Colloid and Interface Science*, *162*(1), 182–188. https://doi.org/10.1006/jcis.1994.1023

[16] Krishna, R., & Long, J. R. (2011). Screening metal–organic frameworks by analysis of transient breakthrough of gas mixtures in a fixed bed adsorber. *The Journal of Physical Chemistry C*, *115*(26), 12941–12950.

[17] Lopes, F. V. S., Grande, C. A., & Rodrigues, A. E. (2011). Activated carbon for hydrogen purification by pressure swing adsorption: Multicomponent breakthrough curves and PSA performance. *Chemical Engineering Science*, *66*(3), 303–317. https://doi.org/10.1016/j.ces.2010.10.034

[18] Suzuki, T., Sakoda, A., Suzuki, M., & Izumi, J. (1997). Adsorption of carbon dioxide onto hydrophobic zeolite under high moisture. *Journal of Chemical Engineering of Japan*, *30*(5), 954–958.

[19] Shao, Y., Zhang, H., & Yan, Y. (2013). Adsorption dynamics of p-nitrophenol in structured fixed bed with microfibrous entrapped activated carbon. *Chemical Engineering Journal*, *225*, 481–488. https://doi.org/10.1016/j.cej.2013.03.133

[20] Escudero, C., Poch, J., & Villaescusa, I. (2013). Modelling of breakthrough curves of single and binary mixtures of Cu (II), Cd (II), Ni (II) and Pb (II) sorption onto grape stalks waste. *Chemical Engineering Journal*, *217*, 129–138. https://doi.org/10.1016/j.cej.2012.11.096

[21] Jribi, S., Miyazaki, T., Saha, B. B., Koyama, S., Maeda, S., & Maruyama, T. (2016). Corrected adsorption rate model of activated carbon–ethanol pair by means of CFD simulation. *International Journal of Refrigeration*, *71*, 60–68.

[22] Askalany, A. A., & Saha, B. B. (2015). Experimental and theoretical study of adsorption kinetics of Difluoromethane onto activated carbons. *International Journal of Refrigeration*, *49*, 160–168.

[23] Dong, F., Lou, H., Kodama, A., Goto, M., & Hirose, T. (1999). The Petlyuk PSA process for the separation of ternary gas mixtures: Exemplification by separating a mixture of CO_2–CH_4–N_2. *Separation and Purification Technology*, *16*(2), 159–166.

[24] Dunham, R. Q. (2012). *Rosin-Rammler distributions in ANSYS fluent*. (No. LA-UR-12-24026). https://doi.org/10.2172/1048829

[25] Kwapinski, W., Winterberg, M., Tsotsas, E., & Mewes, D. (2004). Modeling of the wall effect in packed bed adsorption. *Chemical Engineering & Technology: Industrial Chemistry-*

Plant Equipment-Process Engineering-Biotechnology, *27*(11), 1179–1186.

[26] Natarajan, S., Zhang, C., & Briens, C. (2005). Numerical simulation and experimental verification of gas flow through packed beds. *Powder Technology*, *152*(1–3), 31–40. https://doi.org/10.1016/j.powtec.2005.01.006

[27] Slejko, F. L. (1985). *Adsorption technology: A step-by-step approach to process evaluation and application*. USA: M. Dekker.

[28] Ahn, B. J., Zoulalian, A., & Smith, J. M. (1986). Axial dispersion in packed beds with large wall effect. *AIChE Journal*, *32*(1), 170–174.

[29] Guo, X., & Dai, R. (2010). Numerical simulation of flow and heat transfer in a random packed bed. *Particuology*, *8*(3), 293–299. https://doi.org/10.1016/j.partic.2009.10.005

[30] Riffel, D. B., Belo, F. A., & Leite, A. P. F. (2007). Simulation of a shell-and-tube heat exchanger for solar adsorption chiller. In *Heat SET, Heat Transfer in Component and Systems for Sustainable Energy Technologies*, 1–8.

[31] Wu, Y. X., Wang, X., & Ching, C. B. (2002). Computational fluid dynamics simulation of the adsorption separation of three components in high performance liquid chromatography. *Chromatographia*, *55*(7–8), 439–445. https://doi.org/10.1007/BF02492274

[32] Augier, F., Idoux, F., & Delenne, J. Y. (2010). Numerical simulations of transfer and transport properties inside packed beds of spherical particles. *Chemical Engineering Science*, *65*(3), 1055–1064. https://doi.org/10.1016/j.ces.2009.09.059

[33] Jafari, A., Zamankhan, P., Mousavi, S. M., & Pietarinen, K. (2008). Modeling and CFD simulation of flow behavior and dispersivity through randomly packed bed reactors. *Chemical Engineering Journal*, *144*(3), 476–482. https://doi.org/10.1016/j.cej.2008.07.033

[34] Kopanidis, A., Theodorakakos, A., Gavaises, E., & Bouris, D. (2008). Numerical simulation of fluid flow and heat transfer with direct modelling of microscale geometry. In *Proceedings of the 5th European Thermal-Sciences Conference*, 1–9.

How to Cite: Khan, S., Idrees, M., Mushtaq, M. U., & Hussain, S. (2025). Two-Dimensional Multi-scale Modeling of Fixed Bed Adsorption Column Using Computational Fluid Dynamics Simulation. *Archives of Advanced Engineering Science*, *3*(4), 274–283. https://doi.org/10.47852/bonviewAAES42022781

Appendix

Table A1

a	Surface area of particle
C_i	bulk gas concentration (kg/m^3)
C_p	Particle concentration (kg/m^3)
C_2	Inertial resistance coefficient (m)
D_{md}	Molecular diffusivity (m^2/sec)
D_{pt}	Diameter of particle (m)
D_{CD}	Column dispersion coefficient (m)
K_A	Equilibrium Constant
K_B	Equilibrium Constant
k_i	Mass transfer coefficient (sec^{-1})
$M_{A,B}$	Molecular weight of species (g/mol)
N	Number of Component of gas mixture
P	Pressure (Pa)
q_p	Adsorption rate (mmol/g)
q_s	Maximum adsorption capacity (mmol/g)
R	Universal gas law constant (J/mol.K)
T	Temperature (K)
t	Time (sec)
u	Velocity in axial-direction (m/sec)
v	Velocity in radial-direction (m/sec)
ϵ	Bed Porosity
ρ_g	Density of fluid (kg/m^3)
ρ_p	Particle density (kg/m^3)
μ_g	Viscosity of gas mixture (Ns/m^2)
α	viscous resistance coefficient (m^{-1})
Ω	Collision integral
σ	Lennard-Jones Constant